Journal of Power Sources 230 (2013) 218–224

Contents lists available at SciVerse ScienceDirect

Journal of Power Sources

journal homepage: www.elsevier.com/locate/jpowsour

High-performance binder-free Co–Mn composite oxide supercapacitor electrode

Jamie Gomez, Egwu E. Kalu*

Department of Chemical & Biomedical Engineering, Florida A&M University and Florida State University College of Engineering, Tallahassee, FL 32310, USA

HIGHLIGHTS

- Electroless–electrolytic (EE) synthesis of composite oxide electrocatalysts demonstrated.
- Feasibility of electroless co-deposition of Mn and Co demonstrated.
- Electrochemically stable composite Co–Mn oxide for use in ultracapacitor applications prepared.
- EE prepared Co–Mn oxide yielded both high energy density and high power density in a symmetrical cell set-up.

ARTICLE INFO

Article history:
Received 4 August 2012
Received in revised form
15 December 2012
Accepted 17 December 2012
Available online 24 December 2012

Keywords:
Binder-free
Electroless
Supercapacitor
$MnCo_2O_4$
High energy density
Composite oxide

ABSTRACT

A thin film binder-free Co–Mn composite oxide ($MnCo_2O_4$) electrode was fabricated by using electroless –electrolytic (EE) techniques that is amenable to continuous processing and used for supercapacitor applications. The composite oxide was characterized by XRD, XPS and LIBS. A specific capacitance around 832 F g^{-1} at a scan rate of 20 mV s^{-1} was obtained using cyclic voltammetry (CV) and a nearly rectangular-shaped CV curve observed for the composite oxide. When tested in a symmetrical cell setup, the EE electrode yielded a specific capacitance of 240 F g^{-1} at 74 A g^{-1} with an energy density of 21 Wh kg^{-1} and 51.6 kW kg^{-1} of power density. This work suggests the binder-free Co–Mn composite electrode by the low temperature EE method is a promising candidate for high performing supercapacitors.

© 2012 Elsevier B.V. All rights reserved.

1. Introduction

A supercapacitor is a special type of capacitor with a higher energy density than electrolytic capacitors and uses nano-porous material such as porous metal oxide. The combination of high power capability and good specific energy allows supercapacitors to occupy a functional position between batteries and conventional capacitors [1] with applications in computer power back-up, power electronics and electric vehicles [2]. The electrode material is a key component that determines the supercapacitor's capacity. Traditionally, ruthenium oxide has been the electrode material used in pseudocapacitors but its high cost has put manganese and its oxides which are less costly to more common use. Typical electrodes can be fabricated by cathodic deposition and co-precipitation with use of polymer binders and additives [3–5]. The polymer binder fuses active materials and allows the electrode to adhere to a current collector [6]. However, the polymeric binder material leads to increased resistance and reduced capacitance in the supercapacitor [7]. Hence binder-free electrodes have been investigated and some are fabricated by pulsed laser deposition, by combination of techniques including cathodic electrodeposition with chemical vapor deposition and vacuum filtration with chemical precipitation [8–10].

In this paper, electroless–electrolytic (EE) technique with ability to control both the deposit and oxide thicknesses is demonstrated for binder-free Co–Mn composite oxide and its performance for supercapacitor application is evaluated.

2. Materials and methods

Thin film Co–Mn composite oxide was prepared using woven carbon substrate (Fuel Cell Earth, AvCarbele, 11 Ω-cm electrical resistivity, 99.5% carbon content) which is first catalyzed with

* Corresponding author. Tel.: +1 8504106327; fax: +1 8504106150.
E-mail addresses: eek4012@fsu.edu, ekalu@eng.fsu.edu (E.E. Kalu).

0378-7753/$ – see front matter © 2012 Elsevier B.V. All rights reserved.
http://dx.doi.org/10.1016/j.jpowsour.2012.12.069

a palladium polymer ink and then annealed to allow metal deposition. The details of the preparation of the ink and annealing conditions are given by Kuruganti et al. [11]. For the co-deposition of Co and Mn metal on the carbon substrate, an electroless bath consisting of metal salts $CoSO_4$ (13.6 g L^{-1}) and $Mn(NO_3)_2$ (2.4 g L^{-1}), reducing agent $NaPO_2H_2$ (22.8 g L^{-1}), and chelating agents $CO(NH_2)_2$ (41.6 g L^{-1}), H_3BO_3 (30.24 g L^{-1}), and $C_6H_{11}KO_7$ (2.12 g L^{-1}) was used. The plating conditions were set to a temperature range of 70–80 °C and a pH range of 8.5–9.0 maintained using NH_4OH solution. The electrolessly deposited film thickness was about 5 μm for 3 h of electroless plating time. The electro-oxidation of the co-deposited metal thin film to form Co–Mn composite oxide was achieved in a standard three electrode cell arrangement using a 0.7 M sodium hydroxide–ethanol solution, platinum counter and Ag/AgCl reference electrodes and a potentiostat (Solartron (SI) 1287 instrumentation).

The use of binder-free thin film composite oxide in supercapacitor application was demonstrated for both three-electrode and two-electrode cell arrangements. The three electrode cell arrangement comprised Ag/AgCl reference electrode, a platinum counter electrode and fabricated Co–Mn thin film oxide as the working electrode. The symmetrical two-electrode cell setup consisted of glass fiber separator and fabricated composite oxide electrodes. The electrolyte used was aqueous 0.5 M Na_2SO_4. The supercapacitor was discharged and charged in ambient conditions at room temperature using SI 1287. Zeiss 1540 XB Cross Beam Scanning Electron Microscope (SEM) was used to examine the sample structures and a Q-switched Nd:YAG laser (Quantel, Big Sky Brilliant B, USA) was used for laser-induced breakdown spectroscopy (LIBS) elemental analysis. X-ray diffraction (XRD) was used to characterize the phase of the electrolytically formed oxide and XRD patterns recorded with a Rigaku X-ray Diffractometer using Cu Kα radiation (30 kV, 15 mA) at room temperature. Scanning was performed in a 2θ range from 0° to 90°. The measurements were made with 0.01 and 0.05 degree steps and 1 degree/minute rate. The determination of the chemical states of the synthesized oxides was carried out using a VG Scientific (ESCALAB 250) X-ray photoelectron spectroscopy (XPS) equipment with an Al Kα line radiation source under a base pressure of 2.7×10^{-7} Pa. C 1s photoelectron signal at 284.5 eV was used as reference and for the calibration of charge-shifted spectra.

3. Results and discussion

Fig. 1a shows the SEM image of the electroless Co–Mn composite with a porous soy pod-like arrangement. The observed microstructure suggests a possible high surface area for the deposit – a desirable characteristic of the electrode material to contribute greatly to the fast and reversible faradaic redox reactions for the pseudocapacitance. Fig. 1b shows a LIBS spectrum of the Co–Mn composite deposit where Co I and Mn I intensity lines are shown. This provides evidence of not only the elemental composition of the composite but also for the successful electroless co-deposition of Co and Mn.

Following the electroless deposition step, the Co–Mn composite is subjected to an electrolytic oxidation step wherein the metal composite is converted to the oxide. The XRD pattern of the as synthesized composite oxide is shown in Fig. 1c. All the diffraction peaks can be indexed as face-centered cubic spinel phase with space group *Fd3m* $MnCo_2O_4$ (PDF number: 23-1237). The XRD spectrum have broad and poorly defined peaks centered around 2θ of about 30.93°, 36.05°, 38.13°, 42.3°, 53.71° and 80.6° match the (220), (311), (222), (400), (422) and (444) phase structure of $MnCo_2O_4$, respectively. The broad diffraction peaks indicate the presence of spinel cobaltite nanocrystallites. The surface compositions and chemical states of the synthesized composite oxide were analyzed using XPS. Fig. 1d shows XPS spectra for the composite oxide. The C 1s peak occurring at a binding energy of 284 eV is attributed to graphite [12]. The Co 2p XPS spectra of the spinel cobaltite consists of two main lines with the Co $2p_{3/2}$ at a binding energy of 780 eV and the Co $2p_{1/2}$ at 796 eV with the spin-orbit splitting of ~16.0 eV. The Co $2p_{3/2}$ main line has a shake-up satellite peak located at 786.5 eV with energy separation of ~6.5 eV while the shake-up satellite peak for the Co $2p_{1/2}$ is separated by 7 eV from its main peak. The observed results for the binding energy of the Co 2p main lines are similar for most cobalt oxides and hydroxides such as CoO, Co_2O_3, Co_3O_4 and CoOOH and thus makes it difficult to use only the binding energy information of the Co 2p main lines in determining the oxidation state of the cobalt cations. In agreement with literature, the energy separation between the Co $2p_{3/2}$ and Co $2p_{1/2}$ main lines and their corresponding satellites are 7 and 6.5 eV, respectively [13]. An examination of the Mn 2p spectra showed peaks at binding energies of 642 eV and 653 eV with spin orbit of 11 eV between Mn $2p_{3/2}$ and Mn $2p_{1/2}$ are characteristic of Mn^{+4} oxidation state. A peak at 530 eV for the O 1s peak is related to the characteristic oxide oxygen confirming the presence of oxides. Both the XRD and XPS data support the formation of spinels of $MnCo_2O_4$ through the combination of electroless–electrolytic technique. It is to be noted that in the absence of Mn ions, the technique leads to the formation of Co_3O_4.

The effect of varying the molar ratio of Mn and Co in the electroless bath is illustrated in Table 1. With low Mn:Co (0.138:1) ratio the capacitance of the thin film deposit is very low before oxidation but increases after oxidation. With high (Mn:Co) ratio the capacitance before oxidation is 187 F g^{-1} and increases substantially after oxidation to 281 F g^{-1}. The capacitive behavior of the thin film deposit observed before oxidation for the high Mn:Co is attributed to possible co-deposition of elemental Co with some oxide of manganese during the electroless deposition (first step of the two-step approach) step. Also the increase in capacitance after oxidation for both ratios is due to the formation of thin film composite metal oxide when the thin film composite deposit undergoes the electrolytic oxidation step. The redox reaction mechanism for the pseudocapacitance of the Co–Mn composite oxide is described by Eqn. (1) And (2) as follows

$$MnCo_2O_4 + H_2O + OH^- \rightarrow 2CoOOH + MnOOH + e \quad (1)$$

$$MnOOH + OH^- \rightarrow MnO_2 + H_2O + e \quad (2)$$

These chemical transformations are highly reversible [14]. The high Mn:Co was selected to carry out subsequent capacitance studies. Fig. 2 shows cyclic voltammogram (CV) of before and after electrolytic oxidation step for the low and high Mn:Co ratios in the Co–Mn composite. A nearly rectangular shaped CV loop is observed after electrolytic oxidation and shows the effect of the oxidation on the capacitive nature of the oxidized thin film deposit.

Fig. 3 shows CV curves for different scan rates between 20 and 250 mV s^{-1} for the high Co:Mn composite oxide. It is observed that the CV curves are nearly rectangular shaped for scan rates up to 100 mV s^{-1} and is indicative of the low contact resistance. For higher scan rates of 250 mV s^{-1} or more, the CV curves become oval-shaped. This can be attributed to intensified polarization, fast charge transfer and cation diffusion [4]. Although some equivalent series resistance (ESR) exists in the fabricated composite electrodes, the EE electrodes were tested as prepared without optimization to reduce or minimize the ESR. Further, the CV curves in Fig. 3 show no evidence of an oxidation or reduction peak within the scanned potential range hence suggesting a successful oxide

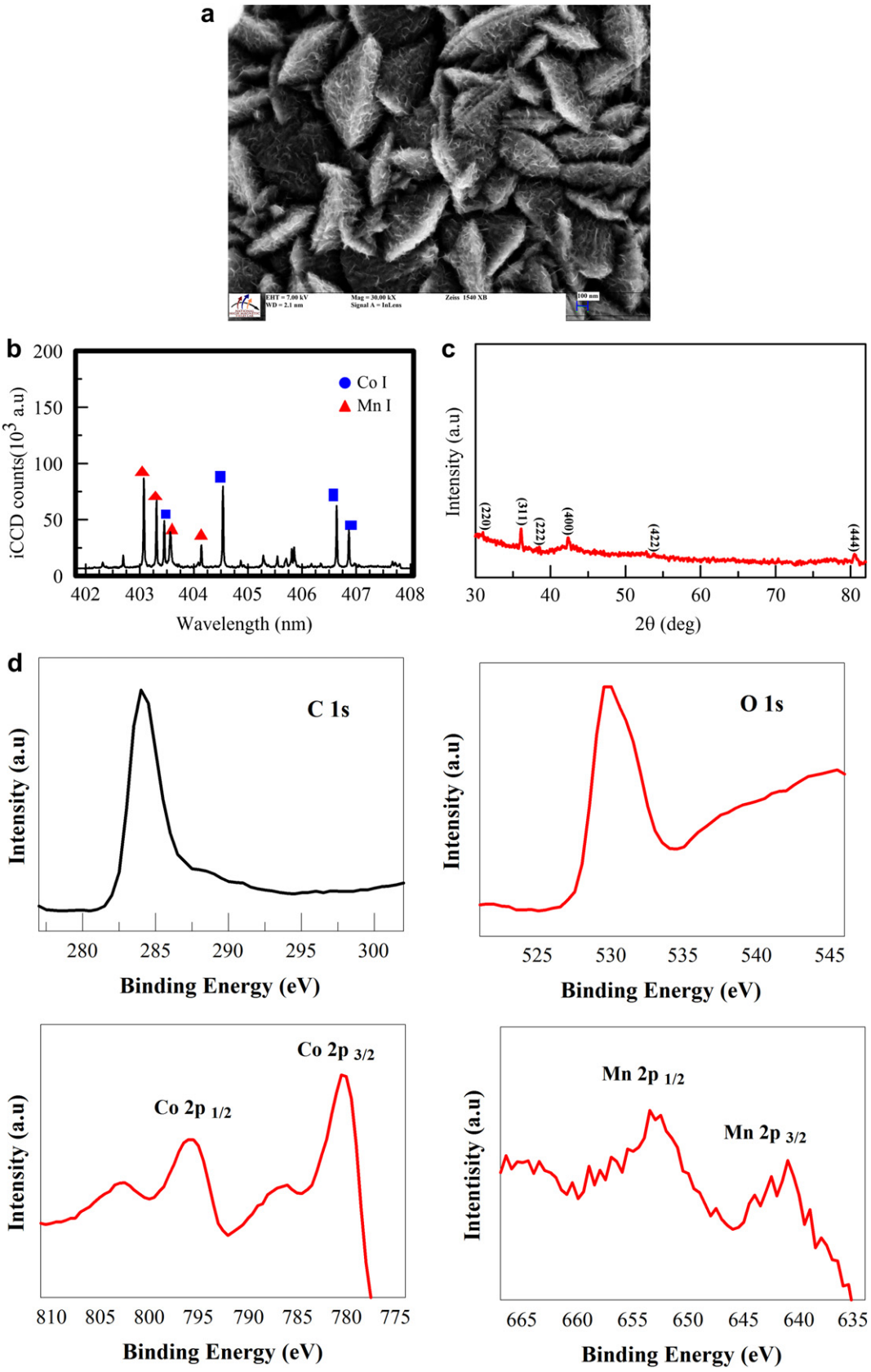

Fig. 1. (a) SEM image for the Co–Mn composite electroless deposit. (b) LIBS spectrum for the high Co–Mn composite electroless deposit. (c) XRD pattern of Co–Mn ($MnCo_2O_4$) composite oxide formed by EE method. (d) High resolution XPS spectra of C 1s, O 1s, Co 2p and Mn 2p regions of the composite oxide.

Table 1
Table showing the effect of electrolytic oxidation on capacitance and electrode performance using varying Mn:Co ratios.

Mn:Co ratio	Capacitance before/ after oxidation F g^{-1}	Energy density Wh kg^{-1}	Power density kW kg^{-1}
0.138:1	Very Low/45.0	4.02	0.92
3.23:1	187.0/281.0	34.8	5.84

formation during the electrolytic oxidation step. The successful high scan rate of 250 mV s^{-1} obtained with the composite oxide suggests a possible application of the electrode for high-power supercapacitors.

Fig. 4a investigates the effect of two electrolytic oxidation times on the oxide capacitance as it varies with scan rate. Specific capacitance ($C_{sp,CV}$) was calculated from cyclic voltammograms as follows

$$C_{sp,CV} = \frac{Q}{\Delta V \times dv/dt \times m} \quad (3)$$

where Q is the area under the CV curve (i.e. $\int I_{(V)}dV$), dv/dt is the scan rate, ΔV is potential window and m is the mass of active material. The mass of the active material or electroless thin film composite was 7.5 mg cm^{-2} and was obtained from the difference in substrate mass measured before and after electroless deposition using a sensitive balance with resolution ±0.001 mg. It is important for the reader to appreciate that carbon substrate in the present work plays a role similar to that of nickel foam in a conventional electrode fabrication in which composite oxide and binder mixture is cast onto the foam substrate. Similar to the nickel substrate, the carbon substrate in the present work is not included mass of the electrochemically active material. For a low scan rate of 20 mV s^{-1} a higher capacitance of 833 F g^{-1} is achieved with the 3 h electrolytic oxidation compared to the 641 F g^{-1} value obtained with 1 h electrolytic oxidation. The relationship between oxidation time and amount of oxide formed is apparent since more metal gets converted to its oxide with increased oxidation time. For the high scan rate of 250 mV s^{-1}, a capacitance value of 354 F g^{-1} is observed for both oxidation times and suggests the usefulness of the electrode at high power densities. Fig. 4b is a Ragone plot obtained

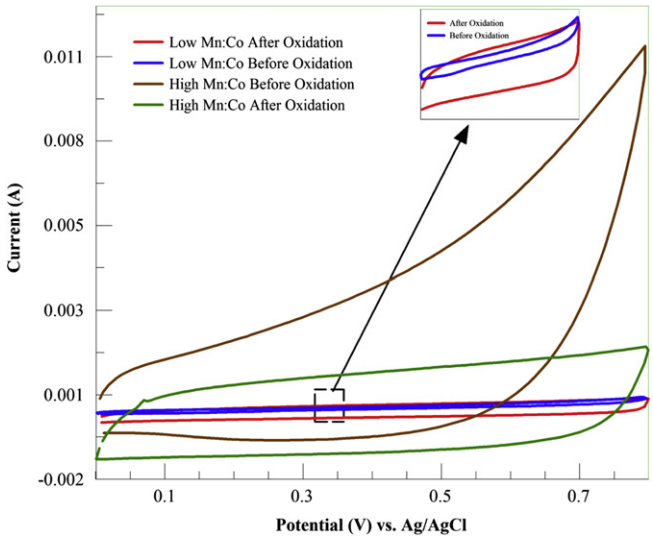

Fig. 2. CV of before and after electrolytic oxidation for the low and high Co–Mn composite oxide carried out in 0.5 M Na_2SO_4 at a scan rate of 50 mV s^{-1}.

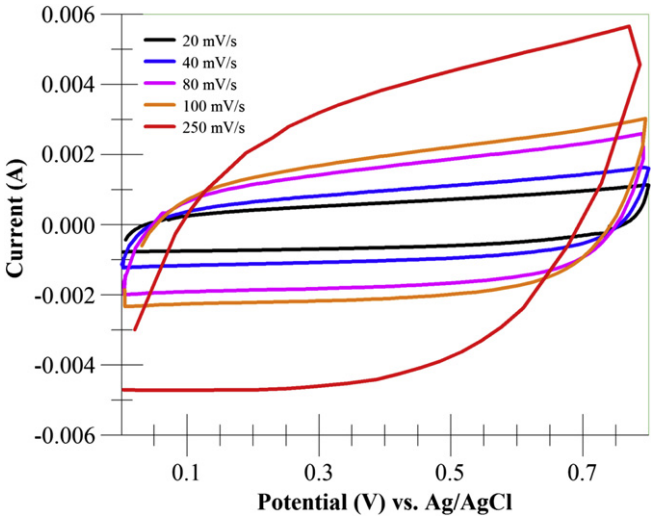

Fig. 3. Comparison of CV curves in 0.5 M Na_2SO_4 for the high Mn:Co composite oxide at different scan rates.

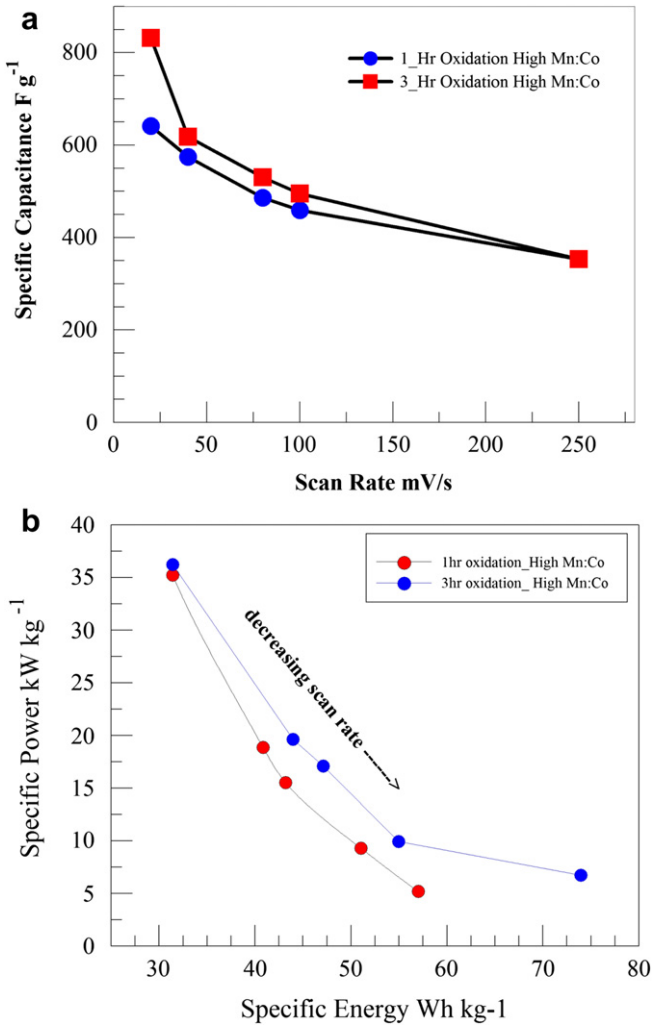

Fig. 4. (a) A plot showing the effect of electrolytic oxidation time on specific capacitance as a function of scan rate for the high Co–Mn composite oxide in 0.5 M Na_2SO_4. (b) Ragone plot obtained based on varying the scan rates for two different electrolytic oxidation times for the high Co–Mn composite oxide.

based on varying the scan rates for the two different electrolytic oxidation times. The energy density (E) and power density (P) of the EE electrode in the Ragone plot were calculated as follows:-

$$E = \frac{C_{sp,CV}\Delta V^2}{2} \quad (4)$$

$$P = \frac{E}{\Delta t} \quad (5)$$

where ΔV is the discharge voltage window, $C_{sp,CV}$ is the specific capacitance and Δt is the discharge time. A high power density (31.4 kW kg^{-1}) and energy density (36 Wh kg^{-1}) at high scan rates is observed for both oxidation times. At lower scan rates, a much higher energy density (73.9 kW kg^{-1}) is observed for the 3-hr oxidation than the 1-hr oxidation time which yielded a much lower energy density (57.1 kW kg^{-1}). The improved energy density observed for the longer oxidation time is attributed to the formation of additional composite oxide. The result demonstrates that both deposition and oxidation times can be used to manipulate the performance characteristics of the supercapacitor fabricated through the EE method.

Fig. 5 shows multiple potential sweeps of the thin film Co–Mn composite oxide with high Mn:Co ratio. It is clear that the CV curves overlap each other and demonstrates the stability of the oxide. Fig. 6 shows the retention of capacitance on cycling after 1000 cycles for the high Mn:Co ratio composite oxide where over 80% of the initial specific capacitance was retained and demonstrates the electrochemical stability of the composite EE electrode.

The previously discussed results reflect operation of the electrodes in a three-electrode cell setup. The performance of the composite oxide was also evaluated in a symmetrical two-electrode cell setup. In the three electrode cell, only one electrode called the working electrode contains the composite oxide material being analyzed and the voltage potential applied to the working electrode is with respect to the reference electrode whereas in the two-electrode cell arrangement, the potential differences applied to each electrode are equal to each other [15]. Fig. 7 compares both cell arrangements and shows that with respect to the two-cell arrangement, a doubling of the capacitance is observed for the three-electrode cell arrangement. This can be attributed to the potential range of the working electrode in a three-electrode cell being twice the potential range in a two electrode cell resulting in a doubling of the calculated capacitance [15].

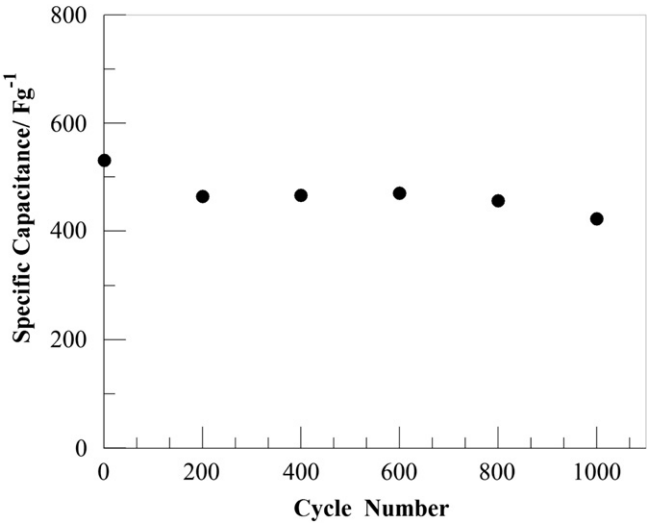

Fig. 6. Specific capacitance versus cycle number plot for the high Co–Mn composite oxide for the three electrode cell setup at 50 mV s^{-1} in 0.5 M Na_2SO_4.

Fig. 8a shows an example galvanostatic charge–discharge curve for the symmetrical supercapacitor using EE electrode at 50 A g^{-1} current density. The applied voltage of the supercapacitor varies near linearly with time and shows good symmetry during charge–discharge for the total range of potential. This gives further evidence of the capacitive behavior of the composite oxide as well as its electrochemical reversibility. The specific capacitance as it varies with cycle number for the two electrode supercapacitor at different current densities is shown in Fig. 8b. The specific capacitance for the symmetrical supercapacitor using EE electrode was calculated as follows

$$C_{sp} = \frac{4 \times I \times \Delta t}{\Delta V \times m} \quad (6)$$

where I is the constant discharge current. For low current densities (6 A g^{-1}), a specific capacitance around 288 F g^{-1} was obtained.

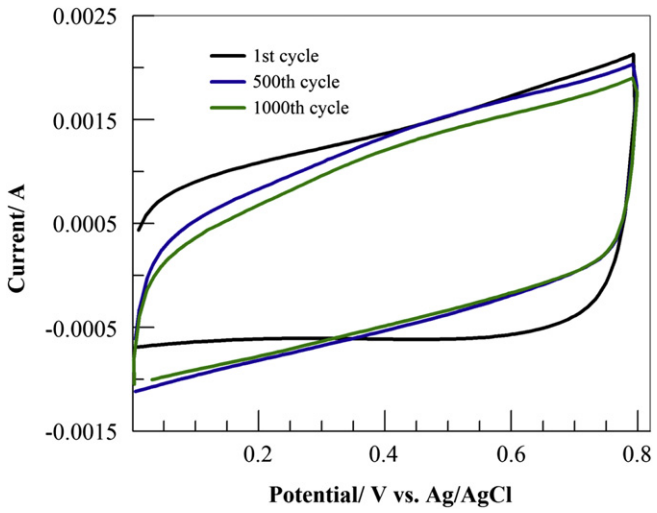

Fig. 5. Multiple potential sweeps in 0.5 M Na_2SO_4 using a three electrode cell setup for the high Co–Mn composite oxide at a scan rate of 20 mV s^{-1}.

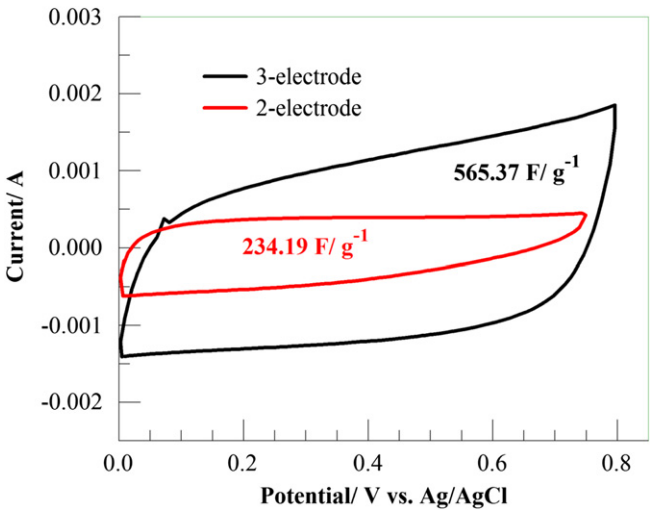

Fig. 7. Comparison of CV curves in 0.5 M Na_2SO_4 for the high Co–Mn composite oxide to evaluate supercapacitor performance in three and two electrode cell setup.

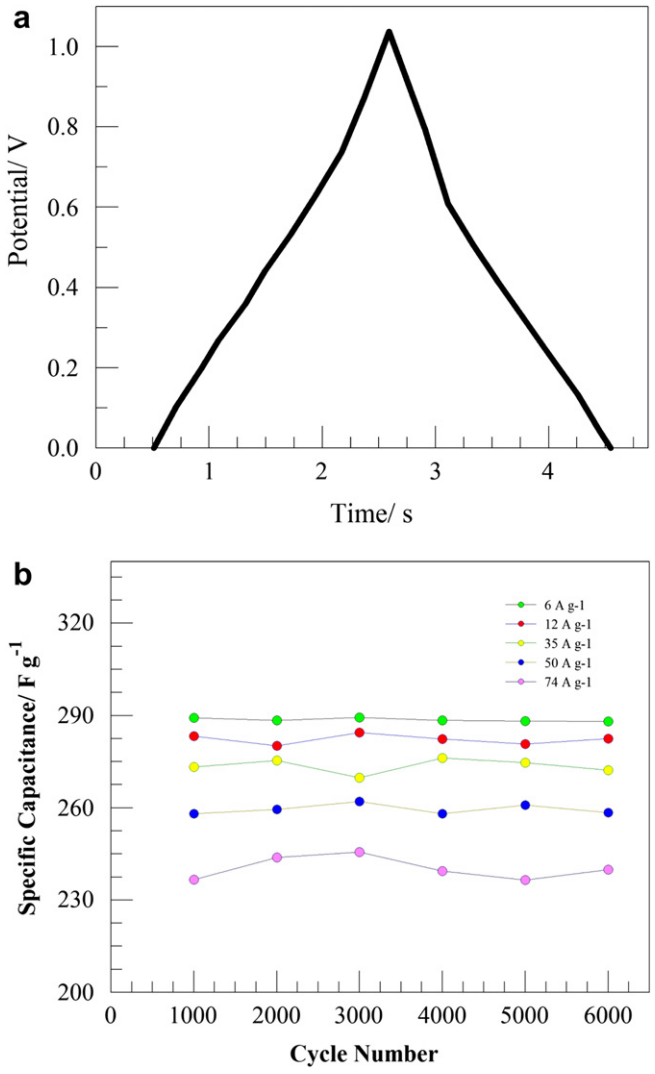

Fig. 8. (a)Charge–discharge curve of the high Co–Mn composite oxide for a symmetrical supercapacitor at a current of 50 A g^{-1} deposit. (b) Specific capacitance versus cycle number showing performance at different current densities for the symmetrical supercapacitor using high Co–Mn composite oxide.

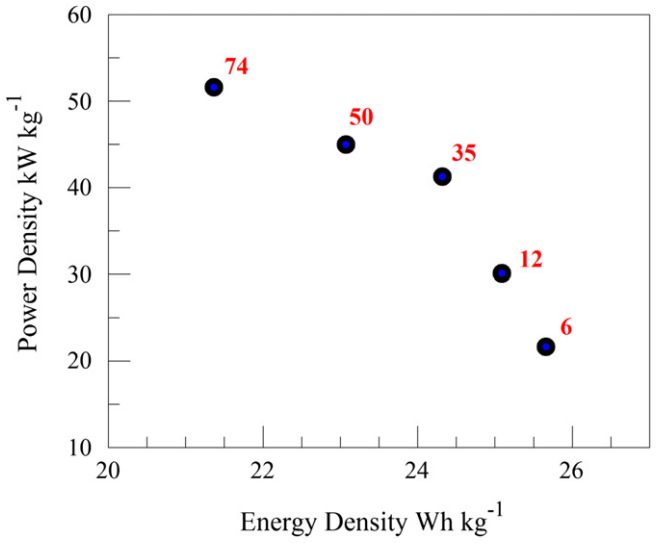

Fig. 9. Ragone plot obtained at various current densities for the symmetrical supercapacitor using high Co–Mn composite oxide.

When the current density is increased from 6 to 74 A g^{-1} a high specific capacitance is still maintained with only a small decrease from 288 to 240 F g^{-1}. This is due to the high rate capability of the thin film Co–Mn composite oxide whose microstructure and binder-free features lead to increased active sites for electrolyte ions. A Ragone plot for the evaluation of the performance of the composite oxide in a symmetrical supercapacitor at different current densities is shown in Fig. 9. At low current density of 6 A g^{-1} the symmetrical cell yielded a high energy density (25.7 Wh kg^{-1}) and power density (21.7 kW kg^{-1}). At even a high current density of 74 A g^{-1}, both a high energy density (25.7 Wh kg^{-1}) and much higher power density (51.6 kW kg^{-1}) is achievable, once again demonstrating that the Co–Mn binder-free electrode prepared by the EE method has stable electrochemical property.

Fig. 10 illustrates the capacity retention of the symmetrical cell at different current densities. The result shows that when the symmetrical cell is cycled up to 6000 cycles, over 95% of its initial discharge capacitance is retained. This shows the potential utility and usefulness of both the thin-film Co–Mn composite oxide and the described EE fabrication method for high power ultracapacitor application and also the electrode's great promise for next generation supercapacitors.

The uniqueness of the EE fabrication approach is its easy amenability to continuous processing. Here, we envision a roll to roll webbing process through which the Pd catalyst ink is coated on the substrate that subsequently passes first through a drying oven and then thermally (or UV) activated and prepared for the electroless deposition step. The Pd coated substrate is then passed through the web into the electroless deposition bath to be plated with desired metal (*s*) wherein the residence time (RT) is used to control the desired deposit thickness. Next, the electrolessly plated substrate is webbed through a rinsing system, dried at set-temperature (e.g. 60 °C) in a stream of hot air and then moved into an electrolytic oxidation bath. Again, the RT in the electrolytic oxidation bath is used to control the thickness of the oxide formed. The electrolessly plated metal is converted to its oxide at constant potential (potentiostatic) condition during the

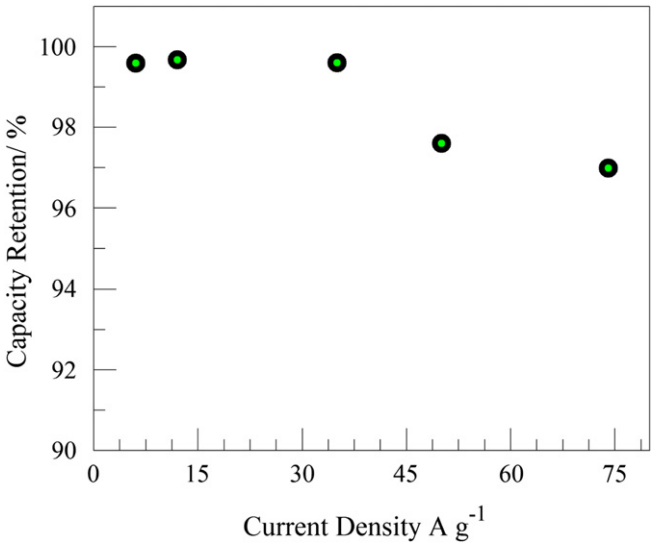

Fig. 10. A plot showing the relationship between capacity retention and current density for the symmetrical supercapacitor using high Co–Mn composite oxide.

oxidation step. The electrolytically oxidized substrate is rinsed and dried and finally annealed at a set temperature and time. The completed binder-free electrode can then be cut into desired shapes dependent on the intended application. The sequence described can be carried out continuously without any break in the sequence. This is fundamentally different from the conventional electrode making technology that involves powder or particle usage with binders and may often be carried out in a batch mode in one of the processing steps.

4. Conclusion

A viable two-step approach for fabricating thin film binder-free composite oxides for supercapacitor applications was developed and illustrated using Co–Mn composite oxide. The Co–Mn composite oxide gave a typical rectangular-shaped CV and a specific capacitance around 460 F g^{-1} at a scan rate of 20 mV s^{-1}. For a symmetrical two-electrode cell the composite electrode yielded a specific capacitance of 273 F g^{-1} at 35 A g^{-1} with an energy density of 24.3 Wh kg^{-1} and 41.3 kW kg^{-1} of power density. The thin film binder-free Co–Mn composite electrode is a promising electrode material for next generation high performing supercapacitors.

Acknowledgments

The work was supported by ERC Program of the National Science Foundation under Award Number EEC-08212121. We would also like to thank Jamal Stephens, FAMU electrical engineering student for his contributions toward this project.

References

[1] P.Y. Chuang, C.C. Hu, J. Mater. Chem. Phys. 92 (2005) 138.
[2] B. Djurfors, J.N. Broughton, M.J. Brett, D.G. Ivey, J. Mater. Sci. 38 (2003) 4817.
[3] J.K. Chang, W.T. Tsai, P.Y. Chen, C.H. Huang, F.-H. Yeh, I.-W. Sun, Electrochem. Solid State Lett. 10 (2007) A9.
[4] R. Jiang, T. Huang, J. Liu, J. Zhuang, Aishui Yu, Electrochim. Acta 54 (2009) 3047.
[5] J.M. Luo, X.G. Zhang, Mater. Res. Bull. 43 (2008) 1119.
[6] N.M. Choi, Y.G. Lee, J.K. Park, J. Power Sources 112 (2002) 61.
[7] H. Zhang, G. Cao, Z. Wang, Y. Yang, Z. Shi, Z. Gu, Nano Lett. 8 (2008) 2664.
[8] D. Yang, J. Power Sources 198 (2012) 416–422.
[9] Y. Wang, H. Liu, X. Sun, I. Zhitomirsky, Scripta Mater. 61 (2009) 1079–1082.
[10] N. Wang, C. Wu, J. Li, G. Dong, L. Guan, ACS Appl. Mater. Interfaces 3 (2011) 4185.
[11] A. Kuruganti, K.S. Chen, E.E. Kalu, Electrochem. Solid State Lett. 2 (1999) 27.
[12] J. Du, P. Zhang, J. Mater. Sci. Technol. 23 (2007) 571.
[13] B.J. Tan, K.J. Klabunde, P.M.A. Sherwood, J. Am. Chem. Soc. 113 (1991) 855.
[14] S.H. Kim, Y.I. Kim, J.H. Park, J. Myoun Ko, Inter. J. Electrochem. Sci. 4 (2009) 1489.
[15] A.G. Pandolfo, A.F. Hollenkamp, J. Power Sources 157 (2006) 11.